Susceptible ferroelectric/antiferroelectric phase transition near the surface of Nb-doped lead zirconate stannate titanate from surface processing

Teng Lu[1], Andrew J. Studer[2], David Cortie[1,2], Kenny Lau[1], Dehong Yu[2], Yujun Feng[3], Hua Chen[4], Zhuo Xu[3], Ray L.Withers[1], Garry J. McIntyre[2] and Yun Liu[1,*]

[1] Research School of Chemistry, The Australian National University, ACT 2601, Australia

[2] Australia Neutron Science and Technology Organization, Lucas Height NSW 2234, Australia

[3] Electronic Materials Research Laboratory, Xian Jiaotong University, Xian 710049, Shaanxi, China

[4] Centre for Advanced Microscopy, the Australian National University, ACT 2601, Australia

KEYWORDS: Antiferroelectrics, ferroelectrics, Neutron diffraction, X-ray diffraction, PFM, PNZST, Surface

ABSTRACT: This work systematically investigated the structure and property of the near-surface and bulk regions of $Pb_{0.99}(Nb_{0.02}Zr_{0.73}Sn_{0.21}Ti_{0.04})O_3$ ceramics using a combination of X-ray and neutron diffraction, piezoelectric force microscopy, and conventional ferroelectric/piezoelectric characterization. It is found that mechanical force can induce an antiferroelectric/ferroelectric phase transition within micrometers of the surface. Such a phase transition is strongly dependent on the processing scenario, leading to differences from the bulk region. This work provides crucial insights into the sensitivity of this class of AFE materials. Clearly surface processing conditions must be taken into account for both accurate structural determination and practical applications.

Antiferroelectric materials, with specific compositions in the ternary $PbZrO_3$-$PbSnO_3$-$PbTiO_3$ system, are widely studied for their promising applications as actuators, sensors as well as in energy storage and electrocaloric devices.[1-6] In terms of the $PbZrO_3$-$PbSnO_3$-$PbTiO_3$ phase diagram[7], materials can exist in an antiferroelectric orthorhombic (AFE_O), an antiferroelectric tetragonal (AFE_T) or a ferroelectric rhombohedral (FE_R) state at room temperature. The resultant state depends strongly but not only upon the chemical composition. It is found that the stability of these antiferroelectric (AFE) and ferroelectric (FE) phases is also very sensitive to external factors, such as applied electric field, mechanical stress and temperature[8-11]. With a composition close to the AFE/FE phase boundary, the appearance of competing phases even strongly depends on the history of processing conditions such as heat-treatment, mechanical pressing and electrical-poling[12-15]. Although such phenomena have been mentioned previously, the whole picture, especially the relation of the structure and property at the near surface region and in the bulk, is still ambiguous.

In this work, we therefore initiate to systematically investigate whether or not the sensitivity of near-surface structure and properties to external conditions extends into the bulk. A $Pb_{0.99}(Nb_{0.02}Zr_{0.73}Sn_{0.21}Ti_{0.04})O_3$ (PNZST) ceramic was thus chosen as an example material for this study. X-ray and neutron powder diffraction (XRPD and NPD, respectively) are employed to distinguish between near-surface (on the micrometer scale) and bulk structure based on the different beam penetration depths[16-17] of X-rays and neutrons. In addition, piezoresponse force microscopy (PFM) and bulk property measurements are used to differentiate between the surface and bulk properties of the material.

$Pb_{0.99}(Nb_{0.02}Zr_{0.73}Sn_{0.21}Ti_{0.04})O_3$ (PNZST) ceramics were prepared by conventional solid state reaction as previously reported[15]. For comparison purposes, four PNZST sample pieces and one powder sample were cut or cracked from the one initial piece of ceramic. The four cut samples have surface sizes of 10 mm × 5 mm and a thickness of ~ 0.8 mm to 1.5 mm depending on processing conditions. The sample 1 was not processed *i.e.* it has a fresh (or as synthesized) surface. The sample 2's surface was polished prior to investigation. The sample 3 was processed in the following way: polishing the surface→ heat-treatment (600 °C for 12 hours). The sample 4 was prepared as follows: polishing the surface→ heat-treatment (600 °C for 12 hours) → re-polishing the surface.

XRPD patterns of samples 1-4 were collected using a PANalytical X'pert Empyrean diffractometer (Cu Kα radiation, 45kV, 40mA). The unit cell parameters were calculated by Le-Bail fitting using pseudo-Voigt profiles (Jana2006)[18-19]. Figure 1a shows the room temperature XRPD patterns of the sample 1-4. All the patterns are indexed based on a parent cubic perovskite structure (labelled with the subscript p). The sample 1 exhibits a non-split and symmetric $(111)_p$ peak as well as an unambiguous 2:1 split in the $(200)_p$ peaks. Additionally, the weak but clear presence of $G\pm1/4(110)_p$ satellite reflections (G denotes parent reflections) such as $1/4(710)_p$, $1/4(714)_p$ and

$1/4(754)_p$ are also observed in the selected peak regions presented in Figure 1b and 1c. This is consistent with antiparallel Pb cation displacements along the pseudo-cubic $[1\text{-}10]_p$ direction, associated with the wave vector $\mathbf{q} = [1/4\ 1/4\ 0]_p^*$, which is in good agreement with the AFE distortion observed in the prototype $PbZrO_3$ (AFE_O structure, space group: *Pbam*)[20]. The refined *Pbam* orthorhombic unit-cell parameters of the sample 1 (calculated by Le-Bail whole pattern fitting) are a = 5.8440(5) Å, b = 11.7045(5) Å and c = 8.1935(5) Å.

The sample 2 again exhibits the 2:1 split $(200)_p$ parent reflections as well as G ± $1/4(110)_p$ satellite reflections, typical for the AFE_O phase. On the other hand, it is evident that both the $(111)_p$ and $(211)_p$ peaks have small shoulders at lower Q values ($Q=4\pi\sin\theta/\lambda$), indicating rhombohedral rather than orthorhombic symmetry. According to the phase diagram[7], the composition of PNZST sample is very close to the junction of three phases (AFE_T, AFE_O and FE_R). The appearance of weak diffraction features associated with rhombohedral symmetry is probably related to a partial structural change from the AFE_O phase (space group, *Pbam*) to the FE_R phase (space group, *R3c*) during the polishing process. The XRPD pattern for the sample 2 indeed suggests the coexistence of AFE_O and FE_R phases. The refined unit-cell parameters assuming a two-phase mixture are a = 5.8447(5) Å, b = 11.7041(5) Å, c = 8.2008(5) Å for the AFE_O phase and a = 4.1330(5) Å, α = 89.78° for the FE_R phase.

The XRPD pattern of the sample 3 differs from the patterns observed in both sample 1 and 2. It shows a single $(200)_p$ peak but clearly-split $(111)_p$ peaks, showing rhombohedral symmetry. In addition, the previously observed G±$1/4(110)_p$ satellite reflections disappear, further suggesting that the 600 °C heat-treatment has induced the phase transition from AFE_O to FE_R. The unit-cell parameters of the FE_R phase in the sample 3 are a = 4.1330(5) Å, α = 89.81°. The XRPD pattern of the sample 4 is very similar to that of the sample 2 *i.e.* it contains a two phase mixture of both AFE_O and FE_R phases.

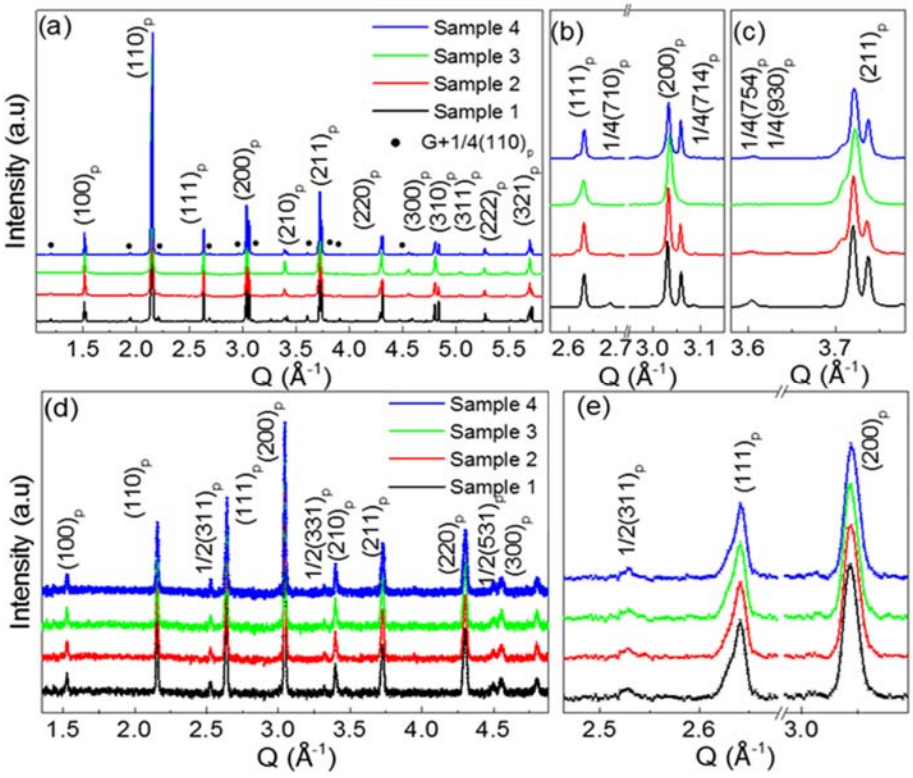

Figure 1. (a) XPRD patterns of samples 1-4, (b) shows details of the region around the parent $(111)_p$ and $(200)_p$ peaks and (c) the $(211)_p$ peaks; and (d) neutron diffraction patterns of the sample 1-4 and (e) the details of the region around $(111)_p$ and $(200)_p$ peaks.

Neutron powder diffraction (NPD) patterns using a wavelength of 2.41 Å were then collected on WOMBAT, the high-intensity powder diffractometer installed on the Opal reactor of the Bragg Institute at the Australian Nuclear Science and Technology Organization. The details of the setup are same as that described in the previous study[17, 21]. The sample stage was rotated anti-clockwise around the normal direction at increments of 15°. An area detector was used for this experiment while each diffraction spectrum was collected for 5 minutes. The 13 patterns collected at the different rotation angles were then averaged. Figure 1d-e shows the resultant NPD patterns for the samples 1-4 along with the associated detail of selected peaks in the 2.46 $Å^{-1}$ < Q < 3.09 $Å^{-1}$ range. This time, there is no obvious difference from one sample to the other. The clearly split $(111)_p$ peaks and unsplit $(200)_p$ peaks are characteristics of the rhombohedral symmetry. In addition to these parent Bragg reflections, G±$1/2(111)_p$ satellite reflections such as $½(311)_p$, $½(331)_p$ and $½(511)_p$ are clearly observed, consistent with the presence of $a^-a^-a^-$ octahedral tilting in Glazer notation[22-23]. Thus the bulk structure of the samples can be assigned to the FE_R phase with *R3c* space group symmetry in a sharp distinction to what is observed for the sample 1, 2 and 4 via XRPD.

As suggested by a previous study[16], the penetration length of low energy X-rays (~ 8 keV) for lead-containing perovskite materials is ~ 10 μm. Because the diffraction geometry of the

lab XRD is reflection, the penetration length is even less at the low incident angles. The differences observed via XPRD and NPD must then result from structural differences between the near-surface and bulk regions of the sample. The fresh near-surface of the sample 1 shows an orthorhombic structure while the bulk structure is clearly rhombohedral. After mechanical polishing, the near-surface of the sample 2 and 4 show a mixture of orthorhombic and rhombohedral phases, indicating that the material surface is very sensitive to the applied mechanical force. For the sample 3, the near-surface, two-phase mixture of orthorhombic and rhombohedral phases induced by polishing is able to revert to a single rhombohedral FE_R phase after heat treatment at 600 °C. Although the average structure of the near-surface region can clearly be tuned by external processing, the average structure of the bulk seems to remain unaffected no matter how the surface is mechanically polished or heat-treated.

The piezoresponse force microscopy (PFM) (Cypher, Asylum Research) was then used to characterize the domain structures of the samples' surfaces. Due to the high roughness of the fresh sample (the sample 1)'s surface, only the sample 2, 3 and 4 were characterized. The polished samples are quite flat (Figure 2a, d and e), excluding the effect of topography on the characterization of the amplitude and phase images. It is found that in both sample 2 and 4, the PFM amplitude and phase images are mostly homogeneous without any obvious contrast. In some areas, however, clear features and contrast was observed.

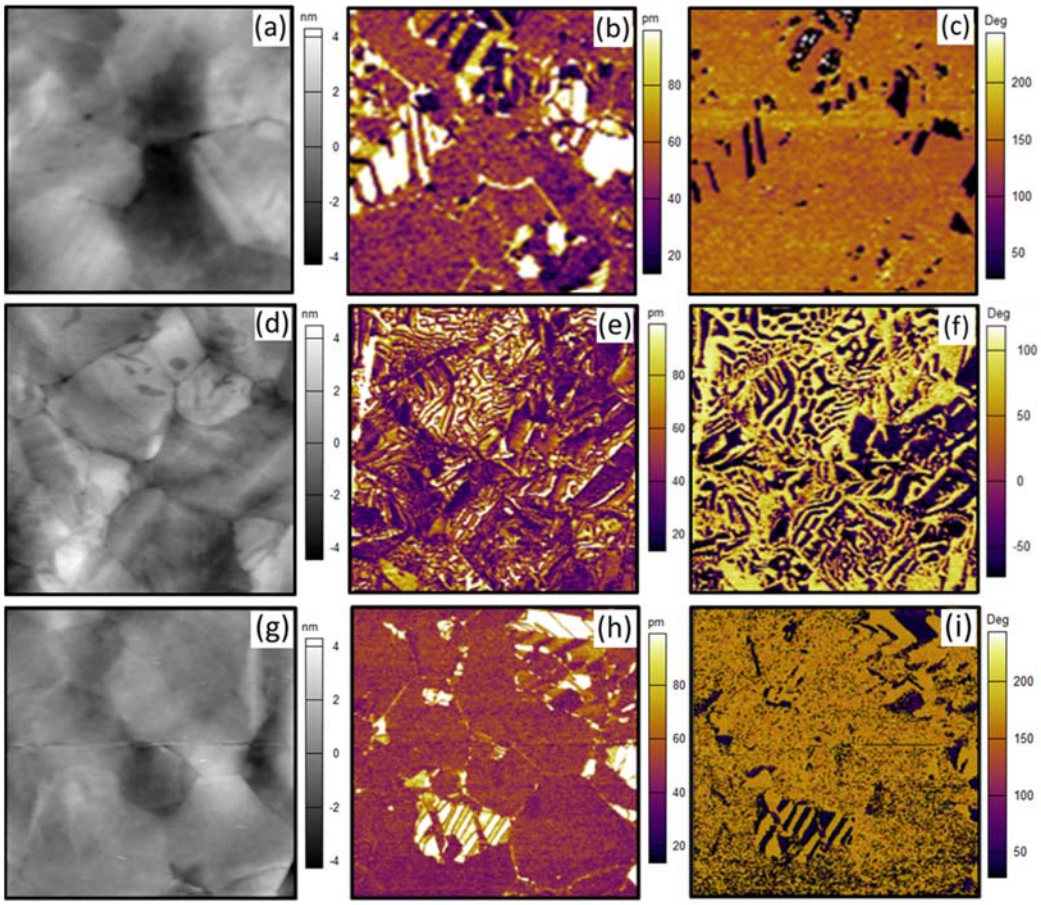

Figure 2 (a, d, g) Morphology, (b, e, h) amplitude and (c, f, i) phase images of the sample 2, 3 and 4, respectively. All scanned areas are 6 μm x 6 μm. The sample 2 and 4 share the similar characters in terms of the amplitude ((b), (h)) and phase images ((c), (i)), indicating the coexistence of the polar and non-polar regions. Different from the sample 2 and 4, most area of the sample 3 exhibits polar domains with a smaller size.

By contrast with the sample 2 and 4, the sample 3 shows sharp features and clear contrast in both amplitude and phase images (Fig.2e and f). Note that the amplitude drops abruptly across domain boundaries while the phase contrast denotes the out-of-plane component of polarization (black and yellow areas correspond to opposite directions of the polarization). Instead of the typical rhombohedral domain structure, the sample 3 shows labyrinthine domains with a size distributed over the range of ~100-200 nm. As suggested by previous studies[24-25], the heat-treatment process releases surface residual strain and minimizes ferroelectric domain sizes. Similarly, in our case, the observed ferroelectric domains become noticeably smaller and their shapes more irregular in the sample 3. Such behavior appears closer to relaxor ferroelectric domain features[26], although structurally the domains still retain the rhombohedral ferroelectric phase.

The PFM results are thus quite consistent with a structural change induced by heat-treatment, whereby a two-phase mixture of AFE and FE near-surface phases are converted to a single FE phase. Interestingly, it is found that the heat-treated

and re-polished FE phase is thereby partially transferred back to AFE again, leading to a combination image showing both FE domains and non-polar regions as observed in the sample 4. That is, mechanical force polishing in the surface region again leads to a partial phase transition from a FE to an AFE phase.

This work shows clearly that the phase structure in the near-surface region of PNZST ceramic samples differs from that of the interior region, and is also easily influenced by external stimuli. The near-surface unit-cell volume of each phase varies accordingly probably due to the different lattice strain induced. Therefore, the origin of the phenomenon is most likely related to a stress/strain induced AFE/FE phase transition[10-11]. As shown in Figure 3, heat-treated powders exhibit a single $(200)_p$ peak in their NPD pattern at ambient pressure (zero hydrostatic pressure), suggesting the FE_R phase. When the powders are under mechanical load (hydrostatic pressure in this case), however, the initially single $(200)_p$ peak splits into two peaks with an unambiguous intensity ratio of 2:1, suggesting the AFE_O phase. This *in-situ* neutron powder diffraction characterization proves that, at this composition, compressive stress stabilizes the AFE phase. The coexistence of the AFE and FE phases in the near surface region of the sample 2 and 4 is thus directly correlated with the mechanical polishing process which changes strain/stress near the surface. By contrast, the sample 3 reverts to the FE_R phase as a result of the relief of surface stress /strain after heat-treatment. As strain induced by polishing only exists near the surface region of ceramics, the bulk material remains in the FE_R phase in regardless of processing conditions.

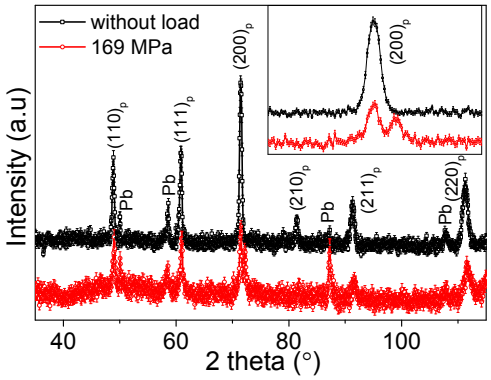

Figure 3. The neutron diffraction patterns of the heat-treated sample powder collected under a hydrostatic pressure of 169 MPa and without pressure.

Figure 4 shows polarization-field (*P-E*) and strain-field (*S-E*) hysteresis loops of the samples 1-4 measured at 1 Hz. Both *P-E* and *S-E* loops of all samples show typical ferroelectric behaviour. Note that, even for the first quarter of the electrical cycle, the observed polarisation shows no trace of AFE behaviour. Although the XRPD patterns of the sample 1, 2 and 4 show a coexistence of AFE and FE phases, the macroscopic FE properties are mainly determined by the bulk structure, which is the FE_R phase. Furthermore, the dielectric properties of these samples were also characterized. All samples present almost identical temperature-dependent dielectric spectra with a sharp dielectric peak at T=169.9 °C (the transition point of the ferroelectric and paraelectric phases) and small variation at T=80 °C (the transition point of the low-temperature ferroelectric phase *R3c* and high temperature ferroelectric phase *R3m*). No additional change in dielectric property is observed from the near surface structure.

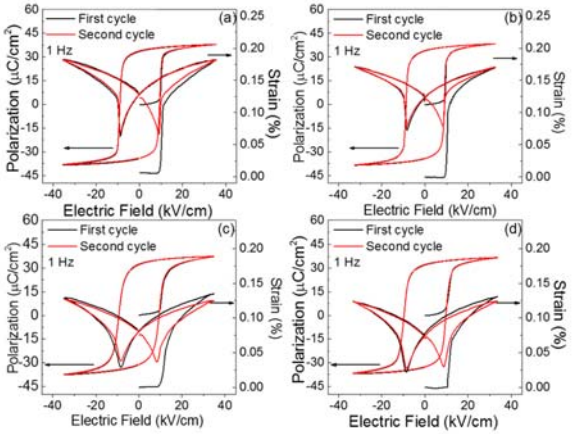

Figure 4. Polarization-electric field (*P-E*) and strain-electric field (*S-E*) hysteresis loops of the (a) sample 1, (b) sample 2, (c) sample 3, and (d) sample 4 measured during first and second electric cycle

In summary, the surface of the PNZST ceramics with chemical composition very close to the AFE/FE phase boundary is quite sensitive to the external stimuli such as mechanical force and temperature. The surface processing therefore results in the difference in both structure and property at the near-surface and in the bulk region. This work thus provides a new insight into AFE polycrystalline materials and AFE/FE phase transitions, suggesting that the considerable complexity of near-surface structures and properties needs to be taken into account to comprehensively understand and control this class of AFE materials as well as their use for specific applications.

AUTHOR INFORMATION

Corresponding Author

*E-mail: yun.liu@anu.edu.au

Author Contributions

TL, AJS, DY collected the neutron data, YF and ZX prepared the ceramic samples, YL applied the beam-time, planned the experiment and supervised the students. TL did all property measurements and analyses. TL, DC, RLW and YL drafted and revised the MP. KL helped measure the PFM. All authors contributed to discussion, data analysis and the manuscript writing.

Notes

The authors declare no competing financial interests.

ACKNOWLEDGMENT

TL, DC, YL and RLW thank the Australian Research Council (ARC) for financial support from in the form of a joint ARC Discovery Project. YL also acknowledges the ARC's support in the form of an ARC Future Fellowship. The authors also thank the Australian Nuclear Science and Technology Organization for support in the form of beam time and postdoctoral fellowship.

REFERENCES

1. Sharifzadeh Mirshekarloo, M.; Yao, K.; Sritharan, T., Large Strain and High Energy Storage Density in Orthorhombic Perovskite $(Pb_{0.97}La_{0.02})(Zr_{1-x-y}Sn_xTi_y)O_3$ Antiferroelectric Thin Films. *Appl. Phys. Lett.* **2010,** *97* (14), 142902.

2. Hao, X.; Yue, Z.; Xu, J.; An, S.; Nan, C.-W., Energy-Storage Performance and Electrocaloric Effect in (100)-Oriented $Pb_{0.97}La_{0.02}(Zr_{0.95}Ti_{0.05})O_3$ Antiferroelectric Thick Films. *J. Appl. Phys.* **2011,** *110* (6), 064109.

3. Ge, J.; Remiens, D.; Dong, X.; Chen, Y.; Costecalde, J.; Gao, F.; Cao, F.; Wang, G., Enhancement of Energy Storage in Epitaxial $PbZrO_3$ Antiferroelectric Films Using Strain Engineering. *Appl. Phys. Lett.* **2014,** *105* (11), 112908.

4. Zhao, Y.; Hao, X.; Zhang, Q., A Giant Electrocaloric Effect of a $Pb_{0.97}La_{0.02}(Zr_{0.75}Sn_{0.18}Ti_{0.07})O_3$ Antiferroelectric Thick Film at Room Temperature. *J. Mater. Chem. C* **2015,** *3* (8), 1694-1699.

5. Peng, B.; Fan, H.; Zhang, Q., A Giant Electrocaloric Effect in Nanoscale Antiferroelectric and Ferroelectric Phases Coexisting in a Relaxor $Pb_{0.8}Ba_{0.2}ZrO_3$ Thin Film at Room Temperature. *Adv. Funct. Mater.* **2013,** *23* (23), 2987-2992.

6. Mischenko, A.; Zhang, Q.; Scott, J.; Whatmore, R.; Mathur, N., Giant Electrocaloric Effect in Thin-Film $PbZr_{0.95}Ti_{0.05}O_3$. *Science* **2006,** *311* (5765), 1270-1271.

7. Berlincourt, D. A., Transducers Using Forced Transitions between Ferroelectric and Antiferroelectric States. *IEEE Trans. Sonics Ultrason* **1966,** *13*, 116.

8. Berlincourt, D.; Krueger, H. H. A.; Jaffe, B., Stability of Phases in Modified Lead Zirconate with Variation in Pressure, Electric Field, Temperature and Composition. *J. Phys. Chem. Solids* **1964,** *25* (7), 659-674.

9. Pan, W.; Zhang, Q.; Bhalla, A.; Cross, L. E., Field-Forced Antiferroelectric-to-Ferroelectric Switching in Modified Lead Zirconate Titanate Stannate Ceramics. *J. Am. Ceram. Soc.* **1989,** *72* (4), 571-578.

10. Avdeev, M.; Jorgensen, J. D.; Short, S.; Samara, G. A.; Venturini, E. L.; Yang, P.; Morosin, B., Pressure-Induced Ferroelectric to Antiferroelectric Phase Transition in $Pb_{0.99}(Zr_{0.95}Ti_{0.05})_{0.98}Nb_{0.02}O_3$. *Phys. Rev. B* **2006,** *73* (6), 064105.

11. Zeuch, D. H.; Montgomery, S. T.; Holcomb, D. J., Uniaxial Compression Experiments on Lead Zirconate Titanate 95/5-2Nb Ceramic: Evidence for an Orientation-Dependent, "Maximum Compressive Stress" Criterion for Onset of the Ferroelectric to Antiferroelectric Polymorphic Transformation. *J. Mater. Res.* **2000,** *15* (03), 689-703.

12. Liu, X.; Tan, X., Suppression of the Antiferroelectric Phase during Polarization Cycling of an Induced Ferroelectric Phase. *Appl. Phys. Lett.* **2015,** *107* (7), 072908.

13. Tan, X.; Frederick, J.; Ma, C.; Aulbach, E.; Marsilius, M.; Hong, W.; Granzow, T.; Jo, W.; Rödel, J., Electric-Field-Induced Antiferroelectric to Ferroelectric Phase Transition in Mechanically Confined $Pb_{0.99}Nb_{0.02}((Zn_{0.56}Sn_{0.43})_{0.94}Ti_{0.06})_{0.98}O_3$. *Phys. Rev. B* **2010,** *81* (1), 014103.

14. Dai, Z.; Xu, Z.; Yao, X., Effect of DC Bias on Pressure-Induced Depolarization of $Pb(Nb,Zr,Sn,Ti)O_3$ Ceramics. *Appl. Phys. Lett.* **2008,** *92* (7), 072904.

15. Frederick, J.; Tan, X.; Jo, W., Strains and Polarization During Antiferroelectric–Ferroelectric Phase Switching in $Pb_{0.99}Nb_{0.02}[(Zr_{0.57}Sn_{0.43})_{1-y}Ti_y]_{0.98}O_3$ Ceramics. *J. Am. Ceram. Soc.* **2011,** *94* (4), 1149-1155.

16. Xu, G.; Zhong, Z.; Bing, Y.; Ye, Z. G.; Stock, C.; Shirane, G., Ground State of the Relaxor Ferroelectric $Pb(Zn_{1/3}Nb_{2/3})O_3$. *Phys. Rev. B* **2003,** *67* (10), 104102.

17. Studer, A. J.; Hagen, M. E.; Noakes, T. J., Wombat: the High-Intensity Powder Diffractometer at the OPAL Reactor. *Phys. B (Amsterdam, Neth.)* **2006,** *385–386, Part 2*, 1013-1015.

18. Le Bail, A., Whole Powder Pattern Decomposition Methods and Applications: A Retrospection. *Powder Diffr.* **2005,** *20* (04), 316-326.

19. Petříček, V.; Dušek, M.; Palatinus, L., Crystallographic Computing System JANA2006: General Features. *Z Krist-Cryst Mater* **2014,** *229* (5), 345-352.

20. Íñiguez, J.; Stengel, M.; Prosandeev, S.; Bellaiche, L., First-Principles Study of the Multimode Antiferroelectric Transition in $PbZrO_3$. *Phys. Rev. B* **2014,** *90* (22), 220103.

21. Lu, T.; Studer, A. J.; Noren, L.; Hu, W.; Yu, D.; McBride, B.; Feng, Y.; Withers, R. L.; Chen, H.; Xu, Z.; Liu, Y., Electric-Field-Induced AFE-FE Transitions and Associated Strain/Preferred Orientation in Antiferroelectric PLZST. *Sci. Rep.* **2016,** *6*, 23659.

22. Glazer, A., Simple Ways of Determining Perovskite Structures. *Acta Crystallogr., Sect. A: Cryst. Phys., Diffr., Theor. Gen. Crystallogr.* **1975,** *31* (6), 756-762.

23. Woodward, P., Octahedral Tilting in Perovskites. I. Geometrical Considerations. *Acta Crystallogr., Sect. B: Struct. Sci* **1997,** *53* (1), 32-43.

24. Schmitt, L. A.; Kungl, H.; Hinterstein, M.; Riekehr, L.; Kleebe, H.-J.; Hoffmann, M. J.; Eichel, R.-A.; Fuess, H., The Impact of Heat Treatment on the Domain Configuration and Strain Behavior in $Pb[Zr,Ti]O_3$ Ferroelectrics. *J. Am. Ceram. Soc.* **2015,** *98* (1), 269-277.

25. Kholkin, A.; Morozovska, A.; Kiselev, D.; Bdikin, I.; Rodriguez, B.; Wu, P.; Bokov, A.; Ye, Z.-G.; Dkhil, B.; Chen, L.-Q.; Kosec, M.; Kalinin, S. V., Surface Domain Structures and Mesoscopic Phase Transition in Relaxor Ferroelectrics. *Adv. Funct. Mater.* **2011,** *21* (11), 1977-1987.

26. Li, Q.; Liu, Y.; Schiemer, J.; Smith, P.; Li, Z.; Withers, R. L.; Xu, Z., Fully-Inverted Piezoresponse Hysteresis Loops Mediated by Charge Injection in $0.29Pb(In_{1/2}Nb_{1/2})O_3$–$0.44Pb(Mg_{1/3}Nb_{2/3})O_3$–$0.27PbTiO_3$ Single Crystals. *Appl. Phys. Lett.* **2011,** *98* (9), 092908.

Table of Contents Graphic